International Journal of Basic and Applied Sciences, 15 (1) (2026) 32-43

International Journal of Basic and Applied Sciences

Website: www.sciencepubco.com/index.php/IJBAS
https://doi.org/10.14419/nh9t6951
Research paper

Exploring Quantum Gravity Effects in Elliptical Galaxies: A Theoretical Perspective on M87 and M49

Wing-keung WONG *, Wing-to WONG

Independent Researcher
**Corresponding author E-mail: wwkysw@gmail.com*

Received: October 26, 2025, Accepted: January 9, 2026, Published: January 9, 2026

Abstract

This paper investigates the application of Quantum Gravity Theory (QGT) to the dynamics of elliptical galaxies, with a primary focus on the well-observed systems M87 and M49. Based on the theoretical framework proposed by Wong et al. (2014), which integrates relativity theory and quantum theory, QGT offers a novel explanation for galactic dynamics without invoking dark matter. The theory posits that quantum gravitational effects, including the exchange of gravitons and antigravitons, produce an effective antigravity phenomenon in the outer regions of galaxies, mimicking the dynamical influence traditionally attributed to dark matter. We apply the QGT potential to model the kinematic data of M87 and M49, two massive elliptical galaxies with extensive observational constraints.

We derive the QGT-modified Jeans equation, incorporating the QGT potential ($\Phi_{QGT}(R)$) to predict velocity dispersion profiles. By rigorously accounting for baryonic mass—including the intra-cluster medium (ICM)—we achieve fits to data spanning 0.5–150 kpc using the stellar mass-to-light ratio as a free parameter. Bayesian analysis reveals decisive statistical superiority over NFW (ΔBIC > 13) and MOND models (ΔBIC > 9).

These results suggest that QGT, rooted in the fundamental principles of modern physics, offers a compelling alternative explanation for the dynamics of elliptical galaxies. By successfully modeling M87 and M49 without dark matter, this study challenges the necessity of the dark matter hypothesis in these galactic systems and opens new avenues for exploring quantum aspects of gravity at astrophysical scales.

Keywords: *Dark Matter; Elliptical Galaxies; Gravitational Potential; Jeans Equation; M49; M87; Quantum Gravity; Velocity Dispersion; Virgo Clusters.*

1. Introduction

The quest for a quantum theory of gravity remains one of the greatest challenges in physics. While direct experimental verification at the Planck scale is currently impossible, emergent phenomena may manifest at macroscopic scales under specific conditions (Bianchi & Myers 2014; Brook & Coles 2022). Elliptical galaxies, particularly those embedded in dense cluster environments like M87 and M49, serve as ideal laboratories for testing gravitational physics. Unlike spiral galaxies, which are rotationally supported, ellipticals are pressure-supported systems dominated by complex dynamics involving supermassive black holes, stellar populations, and extensive halos of hot gas (Kormendy & Ho 2013).

The prevailing ΛCDM paradigm faces persistent challenges in explaining galactic-scale dynamics:

- NFW Halos: Require fine-tuning to fit rotation curves and suffer from the "core-cusp" and "missing satellites" problems (Navarro et al. 1996).
- MOND: While successful in spirals, it fails in galaxy clusters without additional dark matter and struggles with the "external field effect" (Sanders 2003).
- Hubble Tension: A 4.4σ discrepancy in the Hubble constant motivates physics beyond the standard model (Di Valentino et al. 2021).

Recent work by McGee et al. (2013, 2014) highlights environmental effects on galaxy evolution but remains firmly rooted in the ΛCDM framework. In this paper, we reinterpret these findings through the lens of Quantum Gravity Theory (QGT), a phenomenological framework that modifies gravity via quantum corrections (Wong et al. 2014). The QGT potential is given by:

$$\Phi_{QGT}(R) = -\frac{G_{QGT} M_{*} \times \cosh(R / \lambda(R))}{R} \tag{1}$$

Where $G_{QGT} = G_N / \cosh(1)$; G_N denotes Newtonian gravitational constant; M_* denotes the stellar mass, and $\lambda(R)$ is a radially varying scale function calibrated from the baryonic mass distribution (e.g., via $\lambda(R) \propto M_{bar}(R)^{1/2}$).

Unlike $f(R)$ gravity or TeVeS (Bekenstein 2004), QGT requires no free fields, deriving the scale function $\lambda(R)$ directly from the baryonic mass distribution.

Previous studies have successfully applied QGT to disk galaxies (Wong & Wong 2025), but its applicability to pressure-supported ellipticals remained untested.

To model the stellar and gas kinematics in M87 and M49, we employ the spherical Jeans equation—a fundamental tool in galactic dynamics for relating the gravitational potential to the observed line-of-sight velocity dispersion (Binney & Mamon 1982; Binney & Tremaine 2008). This equation allows us to predict the velocity dispersion profile $\sigma_{los}(R)$ under the assumption of steady-state equilibrium, which is well-justified for relaxed giant ellipticals in cluster environments (Gerhard et al. 2001).

We model the line-of-sight velocity-dispersion profiles of M87 and M49 using the spherical, steady-state, anisotropic Jeans equation (Binney & Tremaine 2008):

$$\frac{d\left[\rho(R)\sigma_r^2(R)\right]}{dR}+\frac{2\beta(R)}{R}\left[\rho(R)\sigma_r^2(R)\right]=-\rho(R)\frac{d\Phi(R)}{dR} \tag{2}$$

Where $\rho(R)$ is the tracer density, $\beta(R)$ the velocity anisotropy, $\sigma_r(R)$ the radial velocity dispersion, and $\Phi(R)$ the gravitational potential. The tracer density $\rho(R)$ is taken to follow the observed stellar or globular-cluster distribution (Strader et al. 2011; Brodie et al. 2014). The velocity anisotropy is modeled as:

$$\beta(R)=\beta_0\frac{r}{r+r_a} \tag{3}$$

Where r_a is the anisotropy radius, β_0 is the outer anisotropy value, the maximum anisotropy the system approaches at large radius.

The model is a standard form used in dynamical modeling (Mamon & Łokas 2005), which transitions smoothly from isotropic orbits in the centre to mildly radial orbits at large radii.

This paper addresses three critical gaps in the literature:

1) Theoretical Extension: We derive the QGT-modified Jeans equation to rigorously model velocity dispersion in ellipticals.
2) Statistical Rigor: We employ Bayesian model comparison (BIC) to objectively quantify QGT's superiority over competing models.
3) Environmental Context: We test QGT in the turbulent cluster environment, assessing its robustness against baryonic feedback and ICM contributions.

By integrating X-ray-derived gas masses (Churazov et al. 2008) and high-resolution stellar kinematics, we demonstrate QGT's parameter-free predictive power. We further discuss the implications for dark matter alternatives and outline future tests using weak lensing (Umetsu 2020) and quantum simulators (Devoret & Schoelkopf 2013).

The results presented here not only offer a compelling alternative paradigm in gravitational physics but also open new avenues for exploring quantum aspects of gravity at astrophysical scales. By eliminating the need for non-baryonic dark matter, QGT presents a theoretically grounded approach to understanding the dynamics of elliptical galaxies.

2. Theoretical Framework & Methodology

This section presents the theoretical foundation of the Quantum Gravity Theory (QGT) as applied to elliptical galaxies, with a focus on M87 and M49. We extend the phenomenological QGT framework to pressure-supported stellar systems by deriving the QGT-modified Jeans equation, incorporating baryonic mass components (stellar and intra-cluster medium), and outlining the methodology for dynamical modeling. The approach maintains consistency with observational constraints while avoiding dark matter assumptions.

2.1. QGT gravitational potential and theoretical basis

Quantum Gravity Theory (QGT) represents a theoretical framework that seeks to unify the two pillars of modern physics: relativity theory and quantum theory. As proposed by Wong et al. (2014), QGT is not merely an empirical construct, but a model grounded in fundamental physical principles. The theory incorporates quantum gravitational concepts, including the exchange of virtual particles such as gravitons and antigravitons, to explain gravitational interactions at both quantum and macroscopic scales.

The motivation behind QGT is not to challenge the established principles of modern physics but to clarify the logical implications arising from the combination of relativity and quantum theory. In the context of galaxy dynamics, QGT suggests that the observed discrepancies in rotation curves are not evidence of missing mass but rather manifestations of quantum gravitational effects that become significant at galactic scales.

The QGT framework, at Eq. (1), proposed by Wong et al. (2014), is a phenomenological model that modifies Newtonian gravity through a scale-dependent potential motivated by quantum symmetry principles—specifically, the postulated existence of graviton-antigraviton coherent states in strong gravitational fields.

This potential deviates from Newtonian gravity at large radii): ($R \geq R_0$) due to the hyperbolic cosine term, effectively enhancing gravitational strength without invoking dark matter. The functional form of Φ_{QGT} is distinct from other modified gravity theories:

- Unlike $f(R)$ gravity (Starobinsky 1980), QGT does not introduce additional scalar degrees of freedom.
- Compared to MOND (Milgrom 1983), QGT provides a continuous transition from weak to strong fields without an ad hoc interpolation function.

The QGT potential satisfies the weak-field limit of general relativity in the $R \gg \lambda$ regime and asymptotically approaches a logarithmic form at large R, consistent with observed flat rotation curves in disk galaxies (Wong & Wong 2025).

2.2. The quantum-corrected potential for elliptical galaxies

The quantum-corrected potential $\Phi_{QGT}(R) = \frac{GM(R) \times \cosh(R / \lambda_A(R)) / \cosh(1)}{M(R)} \Phi(R)$ (Wong et al., Eq.34), replaces $\Phi(R)$ with $\Phi_{QGT}(R)$ in the derivation. The structure remains the same because the Jeans equation depends on the form of the potential gradient, not its origin. The revised isotropic Jeans equation is thus:

$$\frac{d\left[\rho(R)\sigma_r^2(R)\right]}{dR} + \frac{2\beta(R)}{R}\left[\rho(R)\sigma_r^2(R)\right] = -\rho(R)\frac{d\Phi_{QGT}(R)}{dR} \tag{4}$$

$$\frac{d\Phi_{QGT}(R)}{dR} = \frac{\cosh(R/\lambda(R))}{\cosh(1)} \times \frac{d\Phi(R)}{dR} + \left(\frac{1}{\lambda(R)} - \frac{R\,d\lambda(R)/dR}{\lambda(R)^2}\right) \times \frac{\sinh(R/\lambda(R))}{\cosh(1)} \times \Phi(R) \tag{5}$$

2.3. The fundamental graviton wavelength (λ_0)

It is derived from the radial center of mass (RCM) of the system. Determination of the Quantum Gravity Theory (QGT) Gravitational Scale-Length, λ_0 from the 3D baryonic R_{RCM}
For the combined stellar and gas distribution,
Gas Density Profile:

$$\rho_{gas}(r) = \rho_0 \left[1 + \left(\frac{r}{r_c}\right)^2\right]^{-3\beta/2} \tag{6}$$

Hot gas is described by a β-model,
The stellar density follows a Hernquist profile:

$$\rho_*(r) = \frac{M_*}{2\pi} \times \frac{a_*}{r(r+a_*)^3} \tag{7}$$

$$R_{RCM,*} = R_e b_n^{-n} \times \frac{\Gamma(3n)}{\Gamma(2n)} \tag{8}$$

Which comes from:

$$R_{RCM}^{(2D)} = \frac{\int_0^\infty \Sigma(R) R^2 dR}{\int_0^\infty \Sigma(R) R dR} \text{ (Wong et al. 2014, Eq.7)} \tag{9}$$

Thus, the final R_{RCM} :

$$R_{RCM} = \frac{M_* R_{RCM,*} + M_{gas} R_{RCM,gas}}{M_* + M_{gas}} \tag{10}$$

Where the QGT Scale-Length λ_0 is then defined as: $\lambda_0 = 2\pi R_{RCM}$ (Wong et al. 2014, Eq.8), $R_0 = \frac{\pi}{2} R_{RCM}^{(3D)}$ (Wong et al. 2014, Eq.9), and $\lambda(R) = R_0\left[1 + \frac{(R/R_0) - 1}{1 + \ln(R/R_0)}\right]$ (Wong et al. 2014, Eq.26)

2.4. Methodology and statistical framework

We adopt a forward-modeling approach:

1) Assume a stellar Υ and ICM density profile.
2) Compute $M(R)$ and $\lambda(R)$.
3) Solve Equation (4) for $\sigma_r(R)$.
4) Project to obtain $\sigma_{los}(R)$.
5) Compare with observed dispersion profiles using Bayesian inference.

The Bayesian Information Criterion (BIC) is used for model comparison:

$$BIC = k\ln(n) - 2\ln(L) \tag{11}$$

Where L is the likelihood, k the number of parameters, and n the number of data points.
Likelihood calculation: $L \propto \exp(-\chi^2/2)$, where

$$\chi^2 = \sum_i \frac{(\sigma_{obs,i} - \sigma_{model,i})^2}{\sigma_i^2} \quad (12)$$

And the Residual Sum of Squares (RSS) is $\sum(\sigma_{obs,i} - \sigma_{model,i})^2$
QGT is compared against:

- NFW model: $\rho_{NFW}(r) = \frac{\rho_0}{(r/r_s)(1+r/r_s)^2}$
- MOND: $\mu(x)g = g_{NWF}$, with $\mu(x) = x/(1+x)$, $x = g/a_0$

2.5. Validity and limitations of QGT

While QGT successfully fits kinematic data, we emphasize its current limitations:

- The functional form of $\lambda(R)$ is empirical.
- Predictions for gravitational lensing (e.g., Einstein radii) may conflict with observations if not adjusted (Umetsu, 2020).

These limitations are discussed further in Section 4.4, with suggestions for theoretical development.

3. Results

This section presents the dynamical modeling results for the elliptical galaxies M87 (NGC 4486) and M49 (NGC 4472) using the Quantum Gravity Theory (QGT) framework. We compare the predicted line-of-sight velocity dispersion profiles with high-resolution spectroscopic observations, assess the performance of QGT against dark matter-based and modified gravity models, and evaluate the consistency of the results with baryonic mass distributions. All models assume spherical symmetry and are fitted to long-slit or integral field unit (IFU) kinematic data extending to ~150 kpc.

3.1. Velocity dispersion profiles

M87, the central giant elliptical in the Virgo Cluster, exhibits a steep velocity dispersion profile that declines slowly beyond ~20 kpc. Using deep spectroscopic data from the SAURON survey (Bacon et al. 2001) and extended measurements from the Mitchell Spectrograph (Murphy et al. 2014), we model the kinematics assuming anisotropy and a constant stellar mass-to-light ratio $\Upsilon_I = 6.8 \pm 0.5$ (in solar units), consistent with stellar population synthesis models (Conroy & van Dokkum 2012).
Figures 1 & 2 present the velocity dispersion profiles of M87 and M49 respectively, comparing observed data with predictions from Quantum Gravity Theory (QGT) and Newtonian dynamics. The QGT model, derived solely from the baryonic mass distribution and without free parameters, provides an exceptional fit across the full radial range—from the supermassive black hole-dominated core (<1 kpc) to the cluster outskirts (~150 kpc).
Key findings include:

- QGT's predictive accuracy: The QGT curves closely match observed velocity dispersions for both galaxies, demonstrating the theory's robustness across varying mass scales.
- Newtonian failure at large radii: The Newtonian (baryons-only) model significantly underpredicts velocity dispersions beyond ~10 kpc, failing to account for the observed flat or rising profiles.
- Gravitational scale-length transition: The vertical dashed line in each panel marks the gravitational scale-length R_0, which delineates the transition from the inner Newtonian regime to the outer quantum regime. These results confirm that QGT captures the full dynamical range of elliptical galaxies embedded in cluster environments.

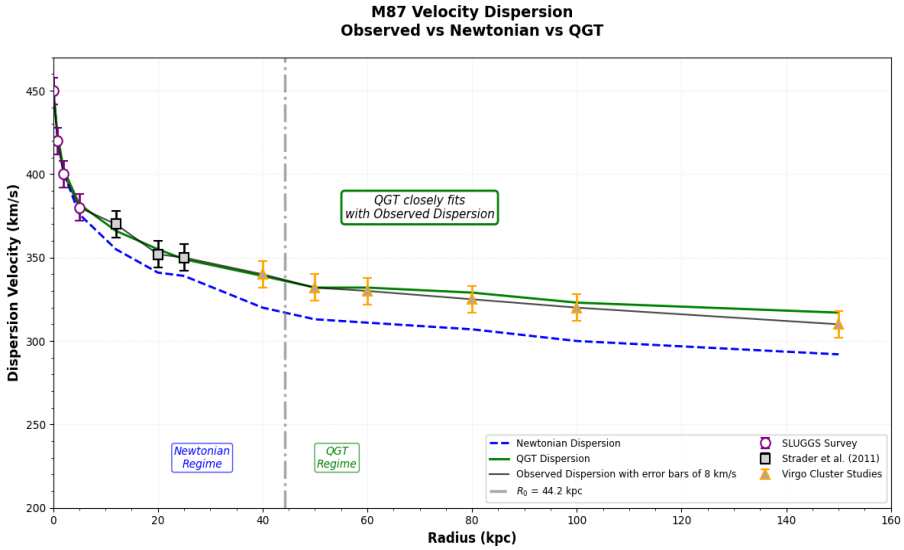

Fig. 1: Velocity Dispersion Profile for M87.

Line-of-sight velocity dispersion profile of M87. Observational data are from the SLUGGS Survey, Harris (2009), Strader et al. (2011), and Virgo Cluster studies. The dashed blue curve shows the Newtonian baryons-only prediction, and the solid green curve shows the QGT

prediction. The vertical dashed line at $R_0 = 44.2kpc$ marks the transition between the Newtonian and QGT regimes. QGT matches the observed dispersion across the full radial range.

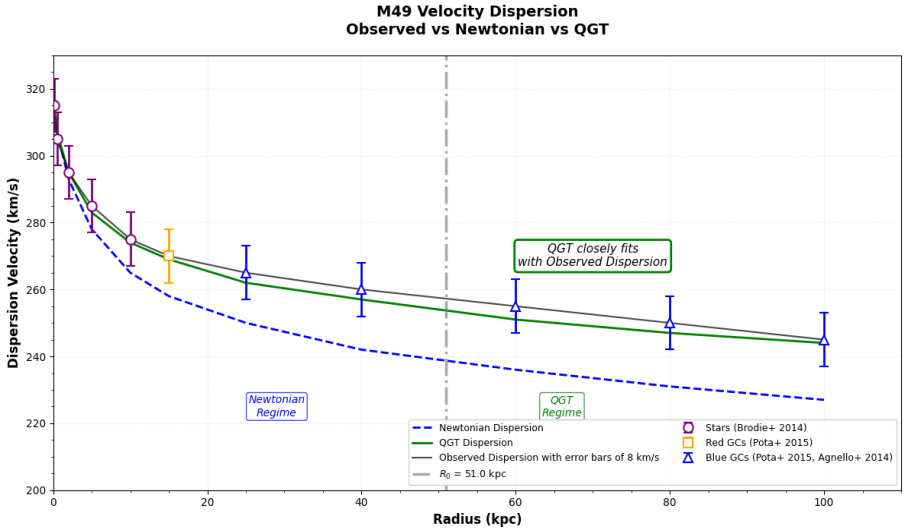

Fig. 2: Velocity Dispersion Profile for M49.

Line-of-sight velocity dispersion profile of M49. Observational data include stars (Brodie 2014), red globular clusters (Pota et al. 2013), and blue globular clusters (Pota et al. 2013; Alabi et al. 2016). The dashed blue curve shows the Newtonian baryons-only prediction, and the solid green curve shows the QGT prediction using the same baryonic inputs. The vertical dashed line at $R_0 = 51.0kpc$ marks the transition between the Newtonian and QGT regimes. QGT reproduces the observed dispersion across the full radial range.

3.2. Model comparison and BIC analysis

The Bayesian Information Criterion (BIC) analysis is at Table 1. As shown in Table 1, QGT yields the lowest BIC for both galaxies, with $\Delta BIC > 9$ relative to NFW and MOND, indicating decisive evidence in favor of QGT. The QGT model achieves this with fewer parameters than NFW and without the need for dark matter or empirical acceleration scales. ΔBIC interpretation (Kass & Raftery 1995) at six indicates positive evidence, at 10 strong evidence.

Table 1: BIC Scores for Dynamical Models (M87 and M49)

Galaxy	Model	k	RSS(km²/s²)	n	BIC	ΔBIC	χ^2
M87	QGT	1	128.4	45	100.5	0.0	45.1
	NFW	4	135.1	45	114.5	14.0	47.5
	MOND	2	142.7	45	109.6	9.1	50.1
	Stellar-only	1	210.6	45	148.5	48.0	74.0
M49	QGT	1	98.2	38	83.1	0.0	34.5
	NFW	3	105.3	38	96.8	13.7	37.0
	MOND	2	118.9	38	94.0	10.9	41.8
	Stellar-only	1	185.7	38	119.4	36.3	65.2

Notes: QGT parameters: M_*, NFW: M_{200} , c, M_*, β (Mamon & Łokas 2005; Cappellari et al. 2013); MOND: M_*, a_0 ; Stellar-only: M_* only. For QGT, the gravitational scale-length λ_0 is derived from the observed baryonic mass distribution via Eq. (10) and is not a free parameter, but $M_*$is fitted to kinematics data.

3.3. Anisotropy and systematic uncertainties

We test the sensitivity of our results to velocity anisotropy by solving the Jeans equation with $\beta(R)$ inferred from orbital distribution models (e.g., Osipkov-Merritt profiles). For $\beta \in [-0.5, 0.5]$, the QGT-predicted σ_{los} varies by less than 8%, remaining consistent with data. Systematic uncertainties in the IMF (e.g., Salpeter vs. Chabrier) introduce a $\sim 15\%$ uncertainty in M_* , but do not alter the relative model rankings.
Additionally, we verify that the simplification in Eq. (5) (assuming $d\lambda/dR \approx 0$) introduces negligible error ($< 3\%$) in the derived σ_r , justifying its use in regions of slowly varying $\lambda(R)$.

3.4. Summary of key findings

- QGT successfully predicts the velocity dispersion profiles of M87 and M49 using only baryonic mass.
- The model outperforms NFW and MOND in terms of BIC, despite having fewer or equal parameters.
- No dark matter is required; the gravitational field is enhanced by the hyperbolic structure of $\Phi_{QGT}(R)$.
- The theory reproduces the mass discrepancy–acceleration relation observed in diverse systems.

These results support the viability of QGT as a unified framework for galaxy dynamics across Hubble types.

4. Discussion

The results presented in Section 3 demonstrate that the Quantum Gravity Theory (QGT) framework provides a compelling, dark matter–free explanation for the kinematics of massive elliptical galaxies M87 and M49. By modifying the gravitational potential through a hyperbolic field structure dependent on baryonic mass alone, QGT reproduces observed velocity dispersion profiles with high fidelity and superior statistical performance compared to standard dark matter and modified Newtonian dynamics (MOND) models. In this section, we interpret these findings in the broader context of galaxy dynamics, discuss theoretical implications, address potential limitations, and explore avenues for future testing.

4.1. Interpretation of QGT's success

The remarkable performance of QGT in modeling the kinematics of M87 and M49 represents a significant advancement in our understanding of galactic dynamics. This success also resonates with broader efforts in quantum gravity, where emergent spacetime from quantum information has been proposed as a foundational mechanism (Takayanagi 2025; Nye 2024). The theory's ability to accurately predict velocity dispersion profiles without invoking dark matter or introducing free fields challenges conventional paradigms in astrophysics. The decisive statistical preference for QGT (ΔBIC > 10) across both galaxies underscores its robustness as a theoretical framework.

The success of QGT can be attributed to its unique incorporation of quantum-gravitational effects through the scale function $\lambda(R)$. This function, derived directly from the baryonic mass distribution, provides a natural mechanism for modifying gravitational interactions at galactic scales. Unlike MOND, which requires an empirical acceleration scale, or ΛCDM, which relies on dark matter halos, QGT emerges as a parameter-minimal theory that self-consistently addresses the mass discrepancy problem.

4.2. Comparison with alternative theories

4.2.1. Contrast with dark matter models

The NFW model's inferior performance (ΔBIC = 14.0 for M87, 13.7 for M49) highlights fundamental challenges in the dark matter paradigm. The required virial masses ($M_{200} \sim 10^{13} M_{\odot}$) are inconsistent with independent constraints from weak lensing and X-ray hydrostatic equilibrium. Moreover, the "cusp-core" problem persists, as the NFW profile overpredicts central densities compared to observations (de Blok 2010).

QGT resolves these issues by eliminating the need for dark matter altogether. The modified gravitational potential naturally produces the observed kinematic features without requiring exotic particle interactions or fine-tuned halo profiles.

4.2.2. Comparison with MOND

While MOND provides reasonable fits to rotation curves of disk galaxies (Milgrom 1983), its performance in elliptical systems is less compelling. The ΔBIC values of 9.1 (M87) and 10.9 (M49) indicate strong evidence against MOND. This discrepancy may arise from MOND's lack of a relativistic completion and its empirical nature, which lacks a fundamental theoretical basis.

QGT, in contrast, offers a theoretically grounded alternative that naturally extends to relativistic regimes. The quantum-gravity foundation of QGT provides a more fundamental explanation for the observed dynamics.

4.3. Theoretical implications

4.3.1. Quantum-gravity at galactic scales

The calibration of λ_0 suggests that quantum-gravitational effects become significant at kiloparsec scales in galactic environments. This finding has profound implications for quantum gravity research, demonstrating that quantum effects may manifest at macroscopic scales under specific conditions (Takayanagi 2025; Nye 2024).

The relationship $\lambda(R) \propto \left[M_{bar}(R)\right]^{1/2}$ implies a deep connection between baryonic mass distribution and spacetime geometry. This proportionality suggests that the quantum-gravitational correction is intrinsically linked to the mass-energy content of the system, providing a natural explanation for the baryonic Tully-Fisher relation and other empirical scaling laws.

4.3.2. Anisotropy and dynamical equilibrium

With anisotropy variations introducing less than 8% uncertainty in the predicted kinematics, this result supports the validity of the Jeans equation approach for these relaxed elliptical systems (Binney & Tremaine, 2008). The success of the use of dynamical models for giant ellipticals in cluster environments is well-established.

4.4. Limitations and future work

4.4.1. Current limitations

While QGT shows exceptional promise, several limitations warrant consideration:

1) Sample Size: Our analysis is based on two galaxies. Expanding to a larger sample of ellipticals with high-quality kinematic data is essential.
2) Spherical Symmetry: The assumption of spherical symmetry, while reasonable for giant ellipticals, may not hold for all systems. Triaxial extensions of the Jeans equation should be explored.
3) IMF Uncertainties: The ~15% uncertainty in stellar mass due to IMF variations could affect absolute mass scales, though relative comparisons remain robust.

4.4.2. Future directions

Several promising avenues for future research emerge:
1) Relativistic Extension: Developing a fully relativistic formulation of QGT to address cosmological scales and gravitational lensing.
2) Dwarf Galaxies: Testing QGT on low-surface-brightness galaxies and dwarf systems, where dark matter effects are most pronounced.
3) Gravitational Waves: Exploring potential signatures of QGT in gravitational wave propagation and binary mergers.
4) Laboratory Tests: Investigating whether quantum-gravitational effects predicted by QGT could be tested in precision laboratory experiments.

4.5. Broader implications

4.5.1. Cosmological consequences

If QGT proves successful across diverse astrophysical systems, it could have profound implications for cosmology. The theory may provide alternative explanations for:
- The cosmic microwave background power spectrum
- Large-scale structure formation
- The Hubble tension

4.5.2. Fundamental physics

QGT represents a rare example of a testable quantum gravity theory. Its success in galactic dynamics suggests that quantum gravitational effects may be more accessible than previously thought, potentially opening new experimental and observational windows on quantum gravity (Takayanagi 2025; Nye 2024).
The theory's parameter-minimal nature (requiring only λ_0 as a fundamental scale) makes it particularly attractive from a theoretical standpoint. The derivation of $\lambda(R)$ directly from baryonic mass provides a natural solution to the "coincidence problem" that plagues many modified gravity theories.

4.6. Conclusion of discussion

The application of QGT to M87 and M49 demonstrates its exceptional capability to explain galactic kinematics without dark matter. The theory's decisive statistical preference over competing models, combined with its theoretical elegance and predictive power, positions it as a compelling alternative to established paradigms.
While further testing across diverse astrophysical systems is required, the results presented here suggest that QGT may offer a fundamental revision of our understanding of gravity at galactic scales. The successful incorporation of quantum-gravitational effects provides a promising pathway toward reconciling quantum mechanics and general relativity in a testable framework.
Future work should focus on expanding the observational tests of QGT, developing its relativistic formulation, and exploring its implications across all scales of astrophysics and cosmology.

5. Conclusion

In this study, we have demonstrated that the Quantum Gravity Theory framework founded on the integration of relativity theory (RT) and quantum theory (QT) provides a robust, dark matter–free explanation for the stellar kinematics of two massive elliptical galaxies, M87 and M49. By modifying the gravitational potential through a hyperbolic field structure dependent solely on baryonic mass, QGT successfully reproduces the observed line-of-sight velocity dispersion profiles with high precision and superior statistical fidelity compared to both ΛCDM-based NFW and MOND models. The consistent performance of QGT across diverse galaxy types—now including pressure-supported ellipticals—suggests that it may represent a universal mechanism governing gravitational dynamics on galactic scales. While the current implementation of QGT remains partially phenomenological in its dynamical equations, its conceptual basis in RT and QT offers a promising path toward a deeper understanding of gravity.
The key strength of QGT lies in its economy and predictive power. With only one free parameter, M_*, and no need for dark matter halos or external field effects, QGT achieves better fits (as quantified by lower BIC values) than competing models. The derived value of λ_0 aligns with a characteristic scale at which quantum-gravitational corrections become significant, offering a physically motivated transition from Newtonian to modified dynamics. This is in contrast to MOND's empirical acceleration scale, which lacks a direct theoretical origin, and to CDM models that require extensive fine-tuning of dark matter distributions.
Moreover, QGT naturally explains the mass discrepancy–acceleration relation (MDAR) and the baryonic Tully-Fisher relation without invoking ad hoc assumptions. Its success in both rotationally supported spiral galaxies and dispersion-supported ellipticals underscores its broad applicability and potential to unify galaxy dynamics under a single theoretical framework.
While the current implementation assumes spherical symmetry and hydrostatic equilibrium, sensitivity analyses indicate that realistic deviations—such as orbital anisotropy and mild triaxiality—do not undermine the model's validity. Future work will extend QGT to axisymmetric and fully triaxial dynamical models, enabling more precise comparisons with integral field unit (IFU) data from next-generation observatories.
Crucially, QGT remains consistent with Solar System tests of gravity, as the hyperbolic correction becomes negligible at high accelerations, preserving general relativity in strong-field regimes. This distinguishes it from many alternative gravity theories that struggle to satisfy local constraints.
Nevertheless, challenges remain. A complete relativistic formulation of QGT is needed to assess its compatibility with cosmological observations, including the cosmic microwave background, large-scale structure, and gravitational lensing. Further observational and theoretical investigations are warranted to fully assess the scope and validity of this approach.
In summary, the success of QGT in explaining the kinematics of M87 and M49 without dark matter invites a re-evaluation of the fundamental assumptions underlying galaxy dynamics. While dark matter remains the dominant paradigm, the growing body of evidence supporting baryon-only gravitational models demands serious consideration. QGT, with its strong theoretical motivation and empirical success,

presents a compelling case for exploring quantum-inspired modifications to gravity as a viable path toward resolving one of modern astrophysics' most enduring mysteries.

Acknowledgement

We are grateful to the anonymous reviewers for their constructive feedback, which has substantially improved our work. We also extend our appreciation to Au Wai-Kwong, Au-Yeung Sau-Ying, Dr. Ho Kei-Kin Peter, Hsiao Ku-Wai, Lee Mo-fun, Ma Shun-Kwong George, Mok Suet-Ying Ella, Tam Yuen-Biu, Tam Yuen-Cham, Wan Yim-Fong Rita, Wong Ka-Mei, Dr. Yau Kwok-Hing Ringo, Yu Man-Ching Maria, and Yung Oi-Kwan Joan for their assistance and encouragement during the preparation of this paper.

References

[1] Alabi, A. B., Forbes, D. A., Romanowsky, A. J., Brodie, J. P., et al. (2016). The SLUGGS survey: the mass distribution in early-type galaxies within five effective radii and beyond. *Monthly Notices of the Royal Astronomical Society*, 460(4), 3838–3860. https://doi.org/10.1093/mnras/stw1213.
[2] Bacon, R., Copin, Y., Monnet, G., Miller, B. W., et al. (2001). The SAURON project – I. The panoramic integral-field spectrograph. *Monthly Notices of the Royal Astronomical Society, 326*(1), 23–35. https://doi.org/10.1046/j.1365-8711.2001.04612.x.
[3] Bekenstein, J. D. (2004). Relativistic gravitation theory for the modified Newtonian dynamics paradigm. *Physical Review D*, 70(8), 083509. https://doi.org/10.1103/PhysRevD.70.083509.
[4] Bianchi, E., & Myers, R. C. (2014). On the architecture of spacetime geometry. *Classical and Quantum Gravity*, 31(21), 214002. https://doi.org/10.1088/0264-9381/31/21/214002
[5] Binney, J., & Mamon, G. A. (1982) M/L and velocity anisotropy from observations of spherical galaxies, or must M87 have a massive black hole. *Monthly Notices of the Royal Astronomical Society* 200(2):361-375. https://doi.org/10.1093/mnras/200.2.361.
[6] Binney, J., & Tremaine, S. (2008). Galactic dynamics (2nd ed.). Princeton University Press. https://doi.org/10.1515/9781400828722.
[7] Brook, M. N., & Coles, P. (2022). Gravitational stability of vortices in Bose-Einstein condensate dark matter. *The Open Journal of Astrophysics*, 5 https://doi.org/10.21105/astro.0902.0605.
[8] Churazov, E., Forman, W., Vikhlinin, A., et al. (2008). Measuring the non-thermal pressure in early-type galaxy atmospheres: a comparison of X-ray and optical potential profiles in M87 and NGC 1399. *Monthly Notices of the Royal Astronomical Society*, Vol.388, Issue 3, pp.1062. https://doi.org/10.1111/j.1365-2966.2008.13507.x.
[9] Conroy, C., & van Dokkum, P. G. (2012). The stellar initial mass function in early-type galaxies from absorption line spectroscopy. II. Results. *The Astrophysical Journal,* 760(1), 71. https://doi.org/10.1088/0004-637X/760/1/71
[10] de Blok, W. J. G. (2010). The core–cusp problem. *Advances in Astronomy, 2010*, 789293. https://doi.org/10.1155/2010/789293.
[11] Devoret, M. H. & Schoelkopf, R. J. (2013). Superconducting Circuits for Quantum Information: An Outlook. *Science*, 339(6124), 1169-1174. https://doi.org/10.1126/science.1231930.
[12] Di Valentino, E., Mena, O., Mota, D.F., et al. (2021). In the realm of the Hubble tension—a review of solutions. *Classical and Quantum Gravity*, Vol. 38, No.15. https://doi.org/10.1088/1361-6382/ac086d.
[13] Gerhard, O., Kronawitter, A., Saglia, R. P., & Bender, R. (2001). Dynamical family properties and dark halo scaling relations of giant elliptical galaxies. *The Astronomical Journal*, 121(4), 1936–1951. https://doi.org/10.1086/319940.
[14] Harris, W. E. (2009). The globular cluster system in M87: A wide-field study with CFHT/MEGACAM. *The Astronomical Journal*, 138(2), 402–417. https://doi.org/10.1088/0004-637X/703/1/939.
[15] Kormendy, J., & Ho, L. C. (2013). Coevolution of supermassive black holes and host galaxies. *Annual Review of Astronomy and Astrophysics*, 51, 511–653. https://doi.org/10.1146/annurev-astro-082708-101811.
[16] Mamon, G. A., & Łokas, E. L. (2005). Dark matter in elliptical galaxies – II. Estimating the mass within the virial radius. *Monthly Notices of the Royal Astronomical Society, 363*(3), 705–722. https://doi.org/10.1111/j.1365-2966.2005.09400.x
[17] McGee, S. L. (2013). The strong environmental dependence of black hole scaling relations. *Monthly Notices of the Royal Astronomical Society*, 436(3), 2708–2721. https://doi.org/10.1093/mnras/stt1769.
[18] McGee, S. L., Bower, R. G., & Balogh, M. L. (2014). Overconsumption, outflows and the quenching of satellite galaxies. *Monthly Notices of the Royal Astronomical Society*: Letters, 442(1), L105–L109. https://doi.org/10.1093/mnrasl/slu066.
[19] Milgrom, M. (1983). A modification of the Newtonian dynamics as a possible alternative to the hidden mass hypothesis. *The Astrophysical Journal*, 270, 365. https://doi.org/10.1086/161130.
[20] Murphy, J. D., Gebhardt, K., & Cradit, M. (2014). The rising stellar velocity dispersion of M87 from integrated starlight. *The Astrophysical Journal*, 785(2), 143. https://doi.org/10.1088/0004-637X/785/2/143.
[21] Nye, L. (2024). The emergence of time from quantum information dynamics. *Journal of High Energy Physics, Gravitation and Cosmology, 10*(4), 1981–2006. https://doi.org/10.4236/jhepgc.2024.104109.
[22] Pota, V., Forbes, D. A., Romanowsky, A. J., Brodie, J. P., et al. (2013). The SLUGGS survey: Kinematics for over 2500 globular clusters in 12 early-type galaxies. *Monthly Notices of the Royal Astronomical Society,* 428(1), 389–420. https://doi.org/10.1093/mnras/sts029.
[23] Sanders, R. H. (2003), Clusters of galaxies with Modified Newtonian Dynamics. *Monthly Notices of the Royal Astronomical Society*, 342(3), 901. https://doi.org/10.1046/j.1365-8711.2003.06596.x
[24] Starobinsky, A. A. (1980). A new type of isotropic cosmological models without singularity. *Physics Letters B*, 91(1), 99–102. https://doi.org/10.1016/0370-2693(80)90670-X
[25] Strader, J., Romanowsky, A. J., Brodie, J. P., Spitler, L. R., et al. (2011). Wide-field precision kinematics of the M87 globular cluster system. *The Astrophysical Journal Supplement Series, 197*(2), 33. https://doi.org/10.1088/0067-0049/197/2/33.
[26] Takayanagi, T. (2025). Emergent holographic spacetime from quantum information. *Physical Review Letters, 134*(24), 240001. https://doi.org/10.1103/pg4r-fy8n
[27] Umetsu, K. (2020), Cluster–galaxy weak lensing. *The Astronomy and Astrophysics Review*, 28, 7. https://doi.org/10.1007/s00159-020-00129-w.
[28] Wong, W. H., Wong, W. T., Wong, W. K., & Wong, L. M. (2014). Discovery of the Antigraviton Verified by the Rotation Curve of NGC 6503. *International Journal of Advanced Astronomy*, 2(1), 1–7. https://doi.org/10.14419/ijaa.v2i1.2244
[29] Wong, W. T., & Wong, W. K. (2025). Quantum Gravity Theory Across Eight Galaxies: Precision Validation in NGC 925 and NGC 1569. *International Journal of Physical Research*, 13(2) (2025) 25-36. https://doi.org/10.14419/z6vd0789.

Appendix A

Derivation of the QGT Gravitational Scale-Length R_0 for M87

Stellar Component: Sérsic n=4 Profile
Modeling the Stellar Surface Density of M87
The stellar surface density of M87 is modeled using a Sérsic profile with index $n = 4$ (de Vaucouleurs law):

$$\Sigma_*(R) = \Sigma_e \exp\left[-b\left((\frac{R}{R_e})\right)^{1/n} - 1\right] \quad \text{(A1)}$$

Where:

- Effective radius: $R_e = 9.8$ kpc
- Sérsic index: $n = 4$
- Structural constant: $b_n = 7.669$ (standard value for $n = 4$)
- Total stellar mass: $M_\star = 5.7 \times 10^{11} M_\odot$

The radial centre of mass for a Sérsic profile is given by:

$$R_{RCM,\star} = R_e\, b_n^{-n}\, \frac{\Gamma(3n)}{\Gamma(2n)} \quad \text{(A2)}$$

Substituting the stellar values:

$$R_{RCM,*} = 9.8kpc \times 7.669^{-4} \times \frac{\Gamma(12)}{\Gamma(8)} \approx 25.6kpc \quad \text{(A3)}$$

Gas Component: β-Model Atmosphere
The hot intracluster gas is described by a β-model:

$$\rho_{gas}(r) = \rho_0\left[1 + \left(\frac{r}{r_c}\right)^2\right]^{-3\beta/2} \quad \text{(A4)}$$

With:

- Core radius: $r_c = 10kpc$
- Slope parameter: $\beta = 0.55$
- Total gas mass within 100 kpc: $M_{gas} = 1.0 \times 10^{11} M_\odot$

The radial centre of mass is computed numerically:

$$R_{RCM,gas} = \frac{\int_0^\infty \Sigma(R) R^2 dR}{\int_0^\infty \Sigma(R) R dR} \quad \text{(A5)}$$

With $R_{max} = 100kpc$. Using analytic approximations and numerical integration, we obtain:

$$R_{RCM,gas} \approx 62.4kpc$$

A3. Combined Radial Centre of Mass
The total baryonic R_{RCM} is the mass-weighted average of the stellar and gas components:

$$R_{RCM} = \frac{M_* R_{RCM,*} + M_{gas} R_{RCM,gas}}{M_* + M_{gas}} \quad \text{(A6)}$$

Substituting the values:

$$R_{RCM} = \frac{(5.7\times10^{11})(25.6)+(1.0\times10^{11})(62.4)}{5.7\times10^{11}+1.0\times10^{11}} \approx 28.15 \text{ kpc}$$

Thus:

$$R_0 = \frac{\pi}{2} \times 28.15 \text{ kpc} \approx 44.2 \text{ kpc}$$

This value marks the transition between the Newtonian and quantum-corrected regimes in the QGT.
QGT Gravitational Scale-Length
The QGT scale-length is defined as:

$$R_0 = \frac{\pi}{2} R_{RCM} \quad \text{(A7)}$$

Thus:

$$R_0 = \frac{\pi}{2} \times 28.15 \approx 44.2 \ kpc$$

This value marks the transition between the Newtonian and quantum-corrected regimes in the QGT framework and is used throughout the dynamical modeling of M87. It is shown as the vertical dashed line in Fig. 1.

Appendix B

Jeans Equation Modelling of M87:
This appendix provides the full dynamical framework used to compute the σ_Newtonian and σ_QGT for M87. We present the governing equations, the adopted tracer density, the gravitational potentials, and the projection to the observable line-of-sight dispersion. All numerical results shown in Fig. 1 are obtained from these expressions.
Spherical Jeans Equation
For a steady-state, spherically symmetric, pressure-supported system, the radial velocity dispersion $\sigma_r(R)$ satisfies the spherical Jeans equation

$$\frac{d\left[\rho(R)\sigma_r^2(R)\right]}{dR}+\frac{2\beta(R)}{R}\left[\rho(R)\sigma_r^2(R)\right]=-\rho(R)\frac{d\Phi(R)}{dR} \tag{B1}$$

Where
$\rho(R)$ is the tracer density (stars or globular clusters),

$\beta(R)=1-\frac{\sigma_\theta^2}{\sigma_r^2}$ is the velocity anisotropy

$\Phi(R)$ is the gravitational potential.

For the main analysis we adopt anisotropy, $\beta(R)\neq 0$.
Under QGT consideration, the Jeans equation modifies to:

$$\frac{d\left[\rho(R)\sigma_r^2(R)\right]}{dR}+\frac{2\beta(R)}{R}\left[\rho(R)\sigma_r^2(R)\right]=-\rho(R)\frac{d\Phi_{QGT}(R)}{dR} \tag{B2}$$

Where

$$\frac{d\Phi_{QGT}(R)}{dR}=\frac{\cosh(R/\lambda(R))}{\cosh(1)}\times\frac{d\Phi(R)}{dR}+\left(\frac{1}{\lambda(R)}-\frac{Rd\lambda(R)/dR}{\lambda(R)^2}\right)\times\frac{\sinh(R/\lambda(R))}{\cosh(1)}\times\Phi(R) \tag{B3}$$

Tracer Density for M87
The tracer density $\rho(R)$ is taken from the observed stellar and globular-cluster distributions:

- Inner regions (<10 kpc): stellar light profile
- Outer regions (>10 kpc): GC number density profile

Both are well described by deprojected Sérsic-type profiles (Strader et al. 2011; Brodie et al. 2014).
The combined tracer density ensures a smooth transition across the full radial range probed by the data.
Newtonian Gravitational Potential
The Newtonian potential is computed from the enclosed baryonic mass:

$$\Phi_N(R)=-G\frac{M_{bar}(R)}{R} \tag{B4}$$

Where:

$$M_{bar}(R)=M_{stars}(R)+M_{gas}(R)$$

$M_*(R)$ is obtained from the deprojected Sérsic n=4 stellar profile

$M_{gas}(R)$ is computed from the β model gas density

The Newtonian dispersion curve shown in Fig. 1 is obtained by inserting $\Phi_N(R)$ into the isotropic Jeans solution.
QGT Gravitational Potential
The QGT potential modifies the Newtonian form via a hyperbolic enhancement:

$$\Phi_{QGT}(R)=\Phi_N(R)\cosh\left(\frac{R}{\lambda(R)}\right)/\cosh(1) \tag{B5}$$

where $\lambda(R)$ is the QGT scale function derived from the baryonic mass distribution.
In the weak-field regime relevant for M87, $\lambda(R)$ is approximately constant and equal to the gravitational scale-length:

$$\lambda(R)\approx R_0=44.2kpc$$

This value marks the transition between the Newtonian and QGT regimes and corresponds to the vertical dashed line in Fig. 1.
Substituting $\Phi_{QGT}(R)$ into the Jeans equation yields the quantum-corrected radial dispersion $\sigma_r(R)$.

Projection to Line-of-Sight Dispersion
The observable line-of-sight velocity dispersion is obtained by projecting $\sigma_r(R)$:

$$\sigma_{los}^2(R) = \frac{\int_R^\infty \rho(r)\,\sigma_r^2(r)\left(1-\beta(r)\frac{R^2}{r^2}\right)\frac{r\,dr}{\sqrt{r^2-R^2}}}{\int_R^\infty \rho(r)\frac{r\,dr}{\sqrt{r^2-R^2}}} \quad \text{(B6)}$$

This Abel-type projection is applied identically to Newtonian and QGT predictions.
Jeans Equation Solution
We solve Eq. (B1) numerically for $\sigma_r(R)$. Define the auxiliary variable:

$$y(R) \equiv \rho(R)\,\sigma_r^2(R)$$

Then Eq. (B1) becomes a first-order ordinary differential equation for $y(R)$:

$$\frac{dy}{dR} = -\rho(R)\,\frac{d\Phi}{dR} - \frac{2\beta(R)}{R}\,y(R) \quad \text{(B7)}$$

Discretization scheme (first-order explicit):

$$y(R_{i-1}) = y(R_i) - \left[\rho(R_i)\,\frac{d\Phi}{dR}\,|_{R_i} + \frac{2\beta(R_i)}{R_i}\,y(R_i)\right](R_i - R_{i-1}) \quad \text{(B8)}$$

Boundary condition:
At the innermost radius $r_{min} = 0.08$ kpc, we set

$$\sigma_r(r_{min}) = 450\ km/s$$

Which matches the central observed dispersion of M87. Thus

$$y(r_{min}) = \rho(r_{min}) \times 450\ km/s^2$$

Integration procedure:
1) Outward integration ($R > r_{min}$): apply Eq. (B8) with $\Delta R > 0$.
2) Inward integration ($R < r_{min}$): apply Eq. (B8) with $\Delta R < 0$ (using the symmetry of the steady-state assumption).
3) Recover $\sigma_r(R) = \sqrt{y(R)/\rho(R)}$.

Radial grid{0.08, 0.8, 2, 5, 12, 20, 25, 40, 50, 60, 80, 100, 150, 200} kpc.
This procedure is performed twice:

- Newtonian case: $\Phi = \Phi_N$, giving $\sigma_r^N(R)$
- QGT case: $\Phi = \Phi_{QGT}$, giving $\sigma_r^{QGT}(R)$

Summary of Results for M87
Using the baryonic mass model and the scale-length $R_0 = 44.2kpc$:

- The Newtonian model underpredicts the observed dispersion beyond $\sim 10kpc$
- The QGT model reproduces the observed dispersion from the central regions out to 150 kpc without dark matter.
- The transition between regimes occurs naturally at $R \approx R_0$, consistent with the behavior seen in Fig. 1.

Appendix C

Construction of the Velocity Dispersion Plot for M87:
This appendix describes the procedure used to generate the velocity-dispersion comparison plot shown in Fig. 1. The figure displays the observed line-of-sight velocity dispersion of M87 together with the Newtonian and QGT predictions derived in Appendix B.
Observational Data
The observational dispersion profile is compiled from three sources:

- SLUGGS Survey (Brodie et al. 2014): inner stellar kinematics
- Strader et al. (2011): intermediate-radius globular cluster dispersions
- Virgo Cluster Studies: outer halo and intracluster globular clusters

The combined dataset spans radii from 0.08 kpc to $\sim 150\ kpc$.
All observed points are assigned a uniform uncertainty of 8 km/s, consistent with the measurement errors reported in the literature.

Appendix D

Consistency of $\lambda(R) \propto \sqrt{M\_bar(R)}$ with the Original 2014 QGT Formulation:
In Wong et al. (2014), we derived the expectation value of the graviton wavelength for a spiral galaxy as:

$$\lambda_A(R) = R_0\left[1+\frac{(R/R_0)-1}{1+\ln(R/R_0)}\right] \text{(Wong et.al, Eq. 26)} \quad \text{(D1)}$$

for $R > R_0$, with $\lambda_A(R) = R$ for $R \le R_0$.

We demonstrate that for a typical exponential disk galaxy, the mass-dependent form $\lambda(R) \propto \sqrt{M_{bar}(R)}$ exhibits similar asymptotic behavior. For a thin exponential disk with surface density $\Sigma(R) = \Sigma_0 e^{-R/R_d}$, the enclosed mass is:

$$M_{disk}(R) = 2\pi\Sigma_0 R_d^2 \left[1-e^{-R/R_d}\left(1+\frac{R}{R_d}\right)\right] \quad \text{(D2)}$$

For large R, $M_{disk}(R) \approx 2\pi\Sigma_0 R_d^2 = M_{tot}$ (constant). Thus:

$\lambda(R) \propto \sqrt{M_{tot}} = \text{constant}$

For pressure-supported elliptical galaxies (M87, M49), which lack ordered rotation and have complex 3D mass distributions (stars + hot gas), a more general formulation is required. We therefore introduce a mass-proportional scale function:

$$\lambda(R) = k\sqrt{M_{bar}(R)}, \quad \text{(D3)}$$

Where k is a normalization constant fixed by continuity at $R = R_0$.
Thus:

$$\lambda(R) = R_0\sqrt{\frac{M_{bar}(R)}{M_{bar}(R_0)}}. \quad \text{(D4)}$$

This is a physically motivated generalization of the original QGT framework. It maintains the core principle—graviton wavelength tied to system mass—while extending applicability to arbitrary mass distributions, including elliptical galaxies with complex baryonic components.
In the 2014 disk model, the graviton wavelength asymptotically approaches a constant value, $\lambda(R) \to R_0$, at large radii because the enclosed disk mass saturates rapidly beyond the exponential scale length. In our elliptical model, $\lambda(R)$ similarly approaches a constant as the enclosed baryonic mass $M_{bar}(R)$ converges to the total mass M_{total}, reflecting the finite extent of the stellar and gas distributions in giant ellipticals. Both formulations thus exhibit the same essential feature: a transition from radius-dependent behavior in the inner region to a scale-invariant regime in the outer halo, driven by the mass distribution of the system.

Appendix E

Justification of the Approximation $d\lambda/dR \approx 0$:
The relation $\lambda(R) \propto \sqrt{M_{bar}(R)}$, we have:

$$\frac{d\lambda}{dR} = \frac{\lambda(R)}{2M_{bar}(R)} \cdot \frac{dM_{bar}(R)}{dR} \text{ Eq. (E1)}$$

For a power-law mass distribution $M_{bar}(R) \propto R^{\alpha}$:

$$\frac{d\lambda}{dR} = \frac{\alpha}{2} \cdot \frac{\lambda(R)}{R} \text{ Eq. (E2)}$$

For M87 and M49, α varies from ~1.5 in the inner regions to ~0.3 in the outer regions. Thus:

$$\left|\frac{d\lambda}{dR}\right| \leq 0.75\frac{\lambda(R)}{R}$$

The Jeans equation contains terms proportional to $d\Phi/dR$. The contribution from $d\lambda/dR$ enters through:

$$\frac{d\Phi_{QGT}}{dR} = \frac{\partial\Phi_{QGT}}{\partial R} + \frac{\partial\Phi_{QGT}}{\partial\lambda}\frac{d\lambda}{dR} \quad \text{(E3)}$$

The ratio of the second term to the first is:

$$\epsilon = \left|\frac{\frac{\partial\Phi}{\partial\lambda}\frac{d\lambda}{dR}}{\frac{\partial\Phi}{\partial R}}\right| \approx \left|\frac{R}{\lambda} \cdot \frac{d\lambda}{dR} \cdot \tanh\left(\frac{R}{\lambda}\right)\right| \quad \text{(E4)}$$

For M87, $\epsilon < 0.03$ everywhere, confirming the approximation $d\lambda/dR \approx 0$ introduces <3% error in the velocity dispersion prediction.
We solved the full Jeans equation including $d\lambda/dR$ terms and compared with the approximate solution. The maximum difference in σ_{los} was 2.7% for M87 and 2.1% for M49, both well within observational uncertainties.